Partially Melted Zone in Aluminum Welds: Solute Segregation and Mechanical Behavior

The liquated material solidifies with severe segregation into a low-strength, low-ductility structure consisting of a solute-depleted ductile phase and a solute-rich brittle eutectic

BY C. HUANG AND S. KOU

ABSTRACT. Aluminum Alloy 2219 was welded by the gas metal arc welding process to study the partially melted zone (PMZ), which is a narrow region immediately outside the fusion zone. Electron probe microanalysis showed severe Cu segregation occurred within the PMZ when the liquated material solidified. Solidification began as a Cu-depleted α phase of about 2 to 3 wt-% Cu and ended as a Cu-rich eutectic, ranging from normal coupled eutectic (α+θ) of 33 wt-% Cu to divorced eutectic (θ) of 53 wt-% Cu. Consequently, α exists as a strip next to the grain boundary (GB) eutectic, and α surrounds large eutectic particles within grains. Microhardness testing revealed the Cu-depleted α was much softer than the eutectic. Tensile testing was conducted perpendicular to the weld, and the PMZ cracked. The maximum load and displacement before failure were both far below those of the base metal before welding. The GB eutectic fractured while the adjacent Cu-depleted α deformed readily under tension. Similarly, large eutectic particles fractured while the surrounding Cu-depleted α deformed. Because large eutectic particles were elongated in the rolling direction, they fractured easily under tension applied in the rolling direction. The maximum load before failure was slightly lower in a weld perpendicular to the rolling direction than in one parallel to it.

Introduction

Aluminum alloys tend to be susceptible to liquation along the grain boundary (GB) and within grains in a very narrow region immediately outside the weld fusion zone called the partially melted zone (PMZ) (Ref. 1). Grain boundary liquation can result in hot cracking during welding (Refs. 1–7) or loss of ductility after welding (Refs. 8–10).

Huang, *et al.* (Ref. 11), recently studied the liquation mechanism in the gas metal arc welds of 2219 aluminum alloy, which is essentially Al-6.3 wt-% Cu. Extensive liquation occurred both along GBs and at locations of large prior-θ particles within grains. Large prior-θ particles refer to large θ particles present in the base metal before welding. Two new findings were of particular significance: the liquation mechanism and the directional solidification behavior of the liquated material.

Liquation is initiated at the eutectic temperature T_E by the eutectic reaction between the θ phase and the α matrix to form liquid eutectic, and is followed by further melting of the α matrix above T_E. Solidification of the liquated material in the PMZ is directional — upward and toward the weld.

The present study focuses on Cu segregation in the PMZ and the response of the PMZ to microhardness testing and tensile testing.

Experimental Procedure

Alloy 2219, a high-strength aluminum alloy, was selected because it is essentially a binary alloy of Al-6.3 wt-% Cu and its solidification is, therefore, easy to understand. The actual composition of the workpiece is Al-6.33% Cu-0.34% Mn-0.13% Fe-0.12% Zr-0.07% V-0.06% Si-0.04% Ti-0.02% Zn by weight. The dimensions of the workpiece were 10 cm x 20 cm x 6.35 mm. The workpiece was welded in the as-received condition of T851 in the 10-cm direction. T8 stands for solution heat treating, cold working, followed by artificially aging, and T51 stands for stress relieving by stretching (Ref. 12).

Gas metal arc welds were made perpendicular and parallel to the rolling direction. The welding parameters were 6.35 mm/s (15 in./min) welding speed, 25.5 V arc voltage, 190 A average current and Ar shielding. The welding wire was a 1.2-mm-diameter wire of Alloy 2319 and the actual composition was Al-6.3% Cu-0.3% Mn-0.18% Zr-0.15% Ti-0.15 Fe-0.10% V-0.10% Si. The wire feed speed was 13.5 cm/s (320 in./min).

The resultant welds were etched with a solution of 0.5 vol-% HF in water to reveal the microstructure by both optical and scanning electron microscopy (SEM). The SEM micrographs were taken with secondary electron images at 15 kV. Electron probe microanalysis (EPMA-WDS) measured the Cu concentration. Back-scattered image photographs were taken at 15 kV and 35 nA. Quantitative analyses and beam scan X-ray (dot) maps were taken at 7 kV to minimize the electron scattering depth penetration.

Microhardness testing was conducted using a Knoop microhardness tester with a 10-g load and a 5-s duration. Tensile testing was conducted perpendicular to the welds with a constant cross-head speed of 0.51 mm/min. Three tensile specimens were tested for each condition and the dimensions are shown in Fig. 1. The reinforcement was left on two specimens, but removed from the third.

KEY WORDS

Alloy 2219
Partially Melted Zone
Grain Boundary Eutectic
Fusion Zone
Liquation
Solute Segregation

C. HUANG and S. KOU are, respectively, Graduate Student and Professor in the Department of Materials Science and Engineering, University of Wisconsin-Madison, Madison, Wis.

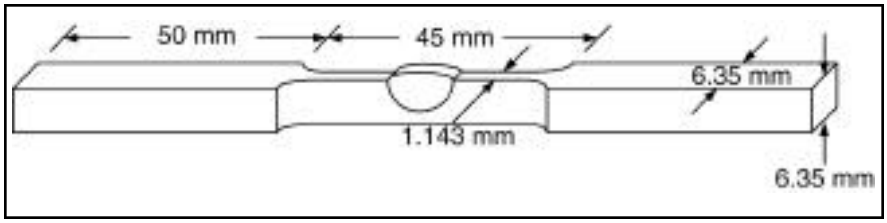

Fig. 1 — Tensile testing specimen.

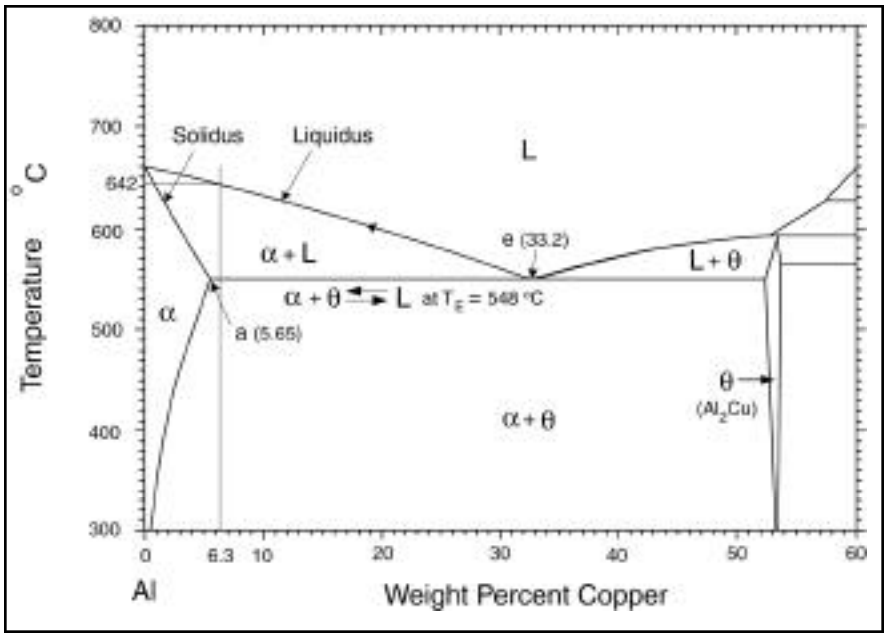

Fig. 2 — Al-Cu phase diagram (Ref. 13).

Results and Discussion

For convenience, the aluminum-rich portion of the Al-Cu phase diagram is shown in Fig. 2 (Ref. 13). Alloy 2219 is considered here as a binary Al-6.3% Cu alloy as an approximation. As shown, the α (Al-rich) phase has a Cu content of up to 5.65%, the eutectic has a Cu/Al weight ratio of about 33/67, and the θ (Al_2Cu) phase has a Cu/Al weight ratio of about 53/47.

Solute Segregation

The specimens for EPMA were not etched in order not to introduce surface-condition-related errors in composition measurements. Consequently, the EPMA micrographs do not have high contrast.

Base Metal

Figure 3 shows the EPMA results of the base metal. The Cu/Al weight ratios of particles 1, 2 and 3 in Fig. 3A are 52.5/45.6, 52.5/44.7 and 53.7/44.4, respectively. These ratios are close to the 53/47 ratio of the θ phase, thus suggesting the particles in the base metal are the θ phase.

Figure 3B shows the Cu concentration distribution along path WX, which cuts across a GB at a small θ particle, and path YZ, which cuts across the same GB without encountering a small θ particle. The maximum Cu concentration along path WX — about 18% — is well below that of 53% for the θ phase, mainly because the electron beam penetrates beyond a small θ particle into the low Cu α matrix. The Cu concentration along path YZ shows the matrix is roughly 6%, and there is no detectable Cu segregation at the GB. In addition to Al and Cu, the concentrations of Mn and Si were also measured. No significant GB segregation of Mn and Si was found.

Edge of the Partially Melted Zone

Figure 4 shows the results of EPMA at the edge of the PMZ facing the base metal, where the peak temperature during welding is the eutectic temperature, T_E. The edge of the partially melted zone was first located by optical microscopy. As will be shown later in Fig. 7, this is the location where the particles change from θ (Fig. 7A) to eutectic — Fig. 7B. The particles in Fig. 4A are on the average larger than those in the base metal — Fig. 3A. The Cu/Al weight ratios of particles 1 and 2 are 39.6/57.6 and 37.6/61.1, respectively. These ratios are much lower than the 53/47 ratio of the θ phase. Both the larger average particle size and the lower Cu/Al ratios suggest these are eutectic particles produced by the eutectic reaction between θ particles and the surrounding α matrix. However, it remains a question why the Cu/Al ratios of these particles are higher than the 33/67 ratio of the eutectic.

From Fig. 4B, again the Cu concentration of the matrix is roughly 6%, and again there is no detectable Cu segregation to the GB, even at a location where the peak temperature during welding is T_E.

Partially Melted Zone

Figure 5 shows the EPMA results in the PMZ. The microstructure is shown in Fig. 5A and enlarged in part in Fig. 5B to indicate the locations of composition measurements. Figure 5C shows the Cu concentration distribution measured along path WX across the GB. Severe segregation of Cu to the GB is evident. The Cu concentration rises from about 2 to 3% in the particle-free strip to a maximum of about 27% at the GB. According to the phase diagram (Fig. 2), the eutectic composition is 33.2% Cu, not 27%. This discrepancy is likely caused by the background effect of the α phase. This part of the GB is thin, about 1.7 μm. In fact, if the overall plane of the GB makes a shallow angle with the top surface of the specimen, this part of the GB can be much thinner than 1.7 μm. The penetration depth of the electron beam in the specimen is likely to be about 1.5 μm at 7 kV, as determined by Monte Carlo simulations with software distributed by Joy (Ref. 15).

Figure 5D shows the Cu concentration distribution measured along path YZ. Severe segregation of Cu to the GB is again evident. The Cu concentration rises from about 2 to 3% in the particle-free strip to a maximum of about 30% at the GB, which is close to the 33% of the eutectic. The discrepancy is smaller here than in the previous case. Since this part of the GB is thicker than the previous one, the effect of beam penetration is likely to be less.

Figure 6 shows EPMA results at an-

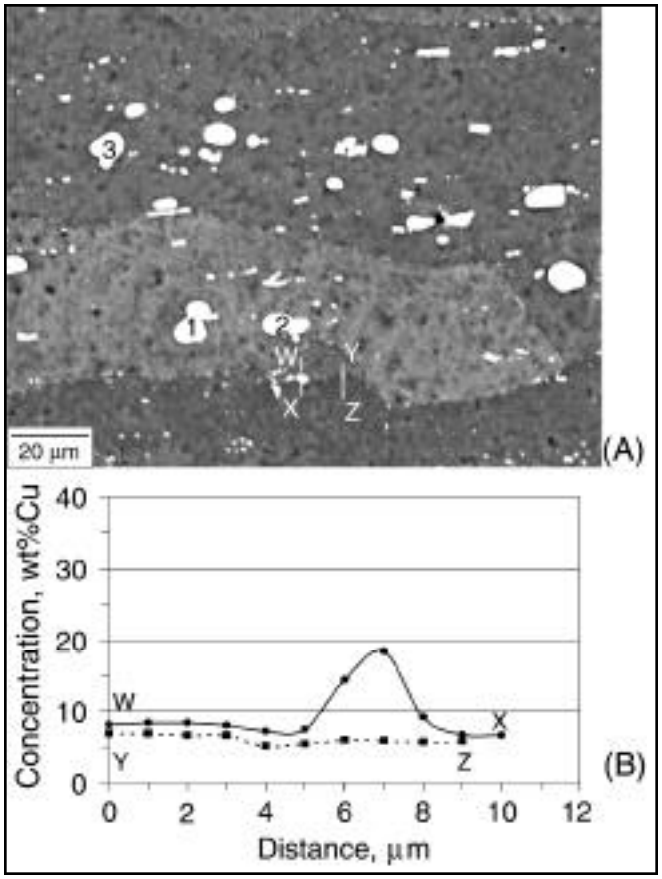

Fig. 3 — EPMA of the base metal: A — Electron micrograph; B — paths WX and YZ across the grain boundary.

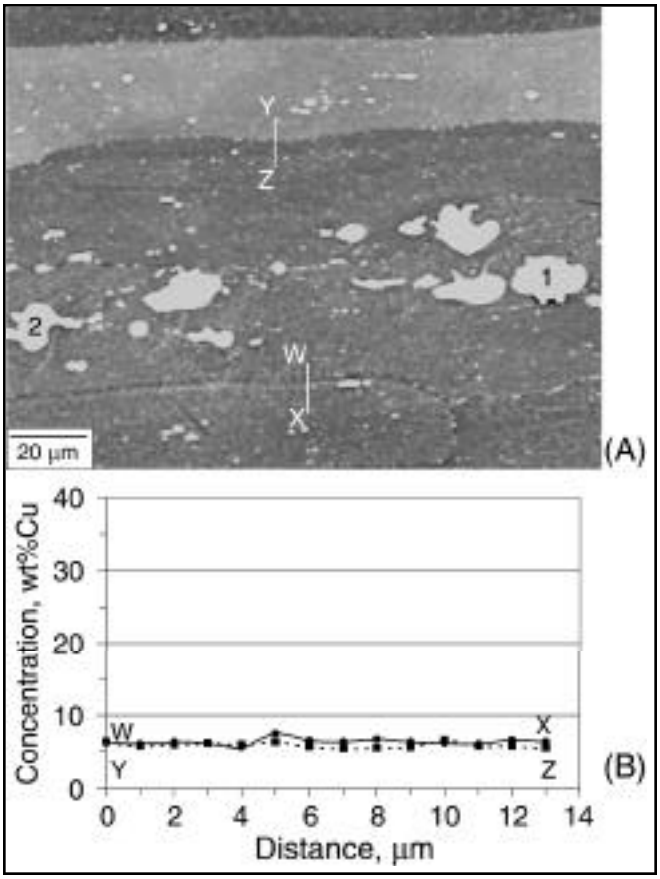

Fig. 4 — EPMA of the edge of the partially melted zone: A — Electron micrograph; B — paths WX and YZ across the grain boundary.

other location in the PMZ. An electron micrograph is shown in Fig. 6A to show the locations of composition measurements. Figure 6B shows the Cu concentration distribution measured along path WX. The maximum Cu concentration is at the GB and is about 33%, which is the eutectic composition. Had point X been extended further into the particle-free strip (like in Fig. 5B), the minimum Cu concentration would have been lower, say 2 to 3%.

Figure 6C shows the Cu concentration distribution measured along path YZ. This time the Cu concentration varies from a minimum about 2 to 3% in the particle-free strip to a maximum of about 55% at the GB and another maximum of about 50% at the particle near point Z. These maximum Cu contents are close to the 53% of the θ phase. The question is why the GB and the particle appear to be θ.

Microstructure

As will be shown, scanning electron micrographs reveal the eutectic structure clearly but not the composition variations in the α phase. Optical micrographs, on the other hand, have limited structural resolution but show the α phase lighter in color where it is depleted in Cu. Therefore, both optical micrographs and scanning electron micrographs are used in the discussion of the microstructure and its relation with the composition data.

The solute segregation shown by EPMA will be discussed in light of the optical micrographs in Fig. 7. Before the discussion, however, it helps to mention that, as shown recently (Ref. 11), the eutectic along the GBs in the PMZ is often divorced. Normal eutectic is typified by the simultaneous growth of α and θ in the normal coupled fashion. In divorced eutectic, however, the α phase of the eutectic grows upon and is, therefore, indistinguishable from the primary α of the matrix, leaving θ alone visible. Divorced eutectic shows no coupling (Ref. 16–21).

Base Metal

As shown in Fig. 7A the large white particles in the base metal are often elongated in the rolling direction (from left to right). According to the phase diagram, 2219 aluminum consists of the α phase and the θ phase. Therefore, these particles should be the θ phase and should have a Cu concentration of about 53%. This is consistent with Cu concentrations of particles 1 through 3 in Fig. 3A.

Edge of the Partially Melted Zone

As already mentioned, near the edge of the PMZ, the maximum peak temperature during welding is the eutectic temperature, T_E. According to the phase diagram, the θ particles react with the surrounding α matrix to form a eutectic liquid.

Figure 7B shows two large eutectic particles near the edge of the PMZ. The one on the right is larger than average and is selected because, in optical micrographs, microstructural details are more clearly seen in larger particles. Both particles consist of divorced eutectic (θ) as well as normal eutectic (α + θ). The divorced eutectic does not appear to be surrounded by the normal eutectic. In fact, it scatters rather than concentrates at the core of the particles, suggesting it is not likely to be the residual of θ particles (like those in Fig. 7A) that have not reacted completely with the surrounding α matrix.

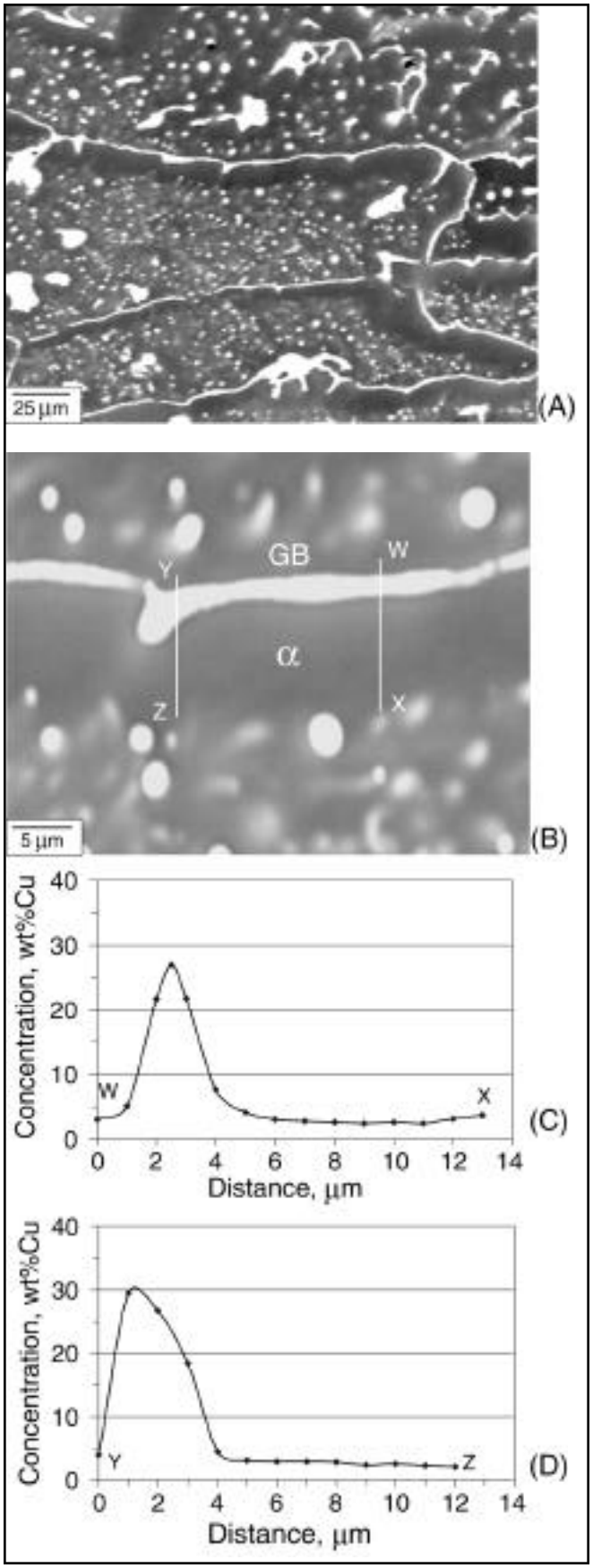

Fig. 5 — EPMA of partially melted zone: A — Electron micrograph; B — electron micrograph at higher magnification; C — path WX across the grain boundary; D — path YZ across the grain boundary.

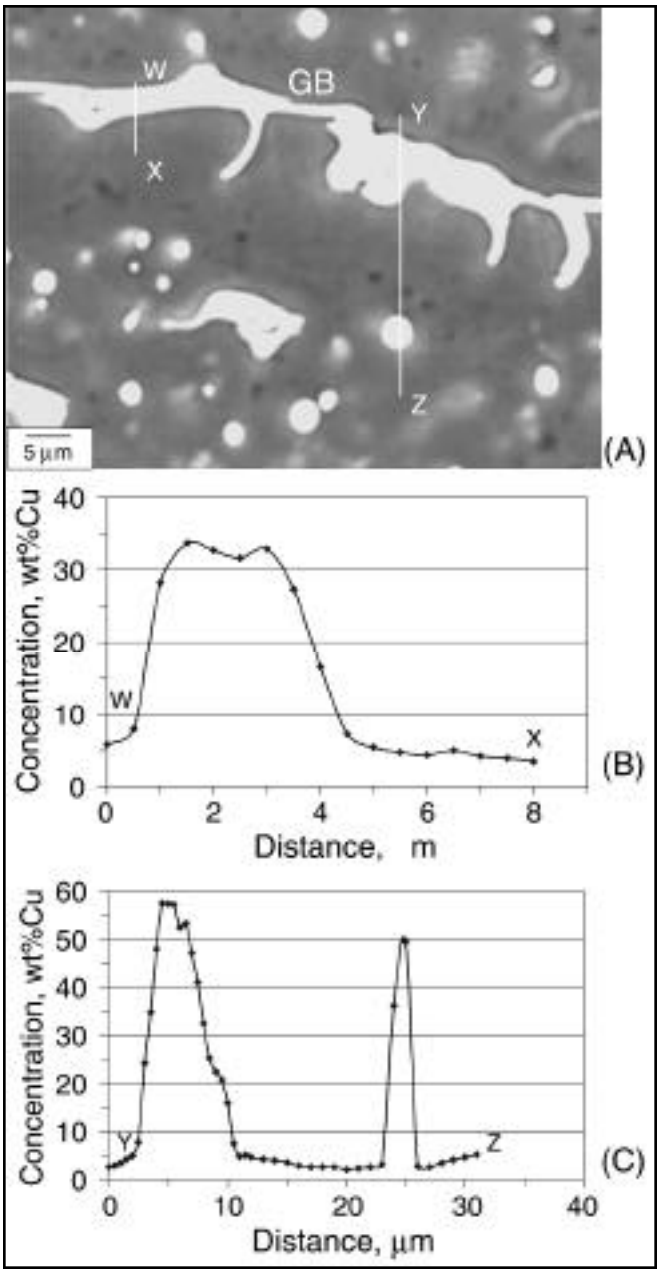

Fig. 6 — EPMA of partially melted zone: A — Electron micrograph; B — path WX across the grain boundary; C — path YZ across the grain boundary.

The same two eutectic particles are shown in the SEM micrographs in Fig. 8A, B. Again, they appear to consist of coupled eutectic (α + θ) and divorced eutectic (θ). The Cu contents of the eutectic particles containing some divorced eutectic (θ) are expected to be higher than 33% because θ has 53% Cu. This makes it possible for the eutectic particles near the edge of the PMZ, such as particles 1 and 2 in Fig. 4A, to have more than 33% Cu.

It is interesting to note in Fig. 8A that some thin but nearly continuous θ is present along parts of the GBs (it appears as dark lines along the GBs in Fig. 7B). This is clear evidence the small θ particles scattered along the GBs before welding (Ref. 11) have reacted with the surrounding α to become eutectic liquid films. Upon cooling, the GB films solidify as divorced eutectic (θ). It is also interesting to note in Figs. 7B, 8A and 8B, the eutectic

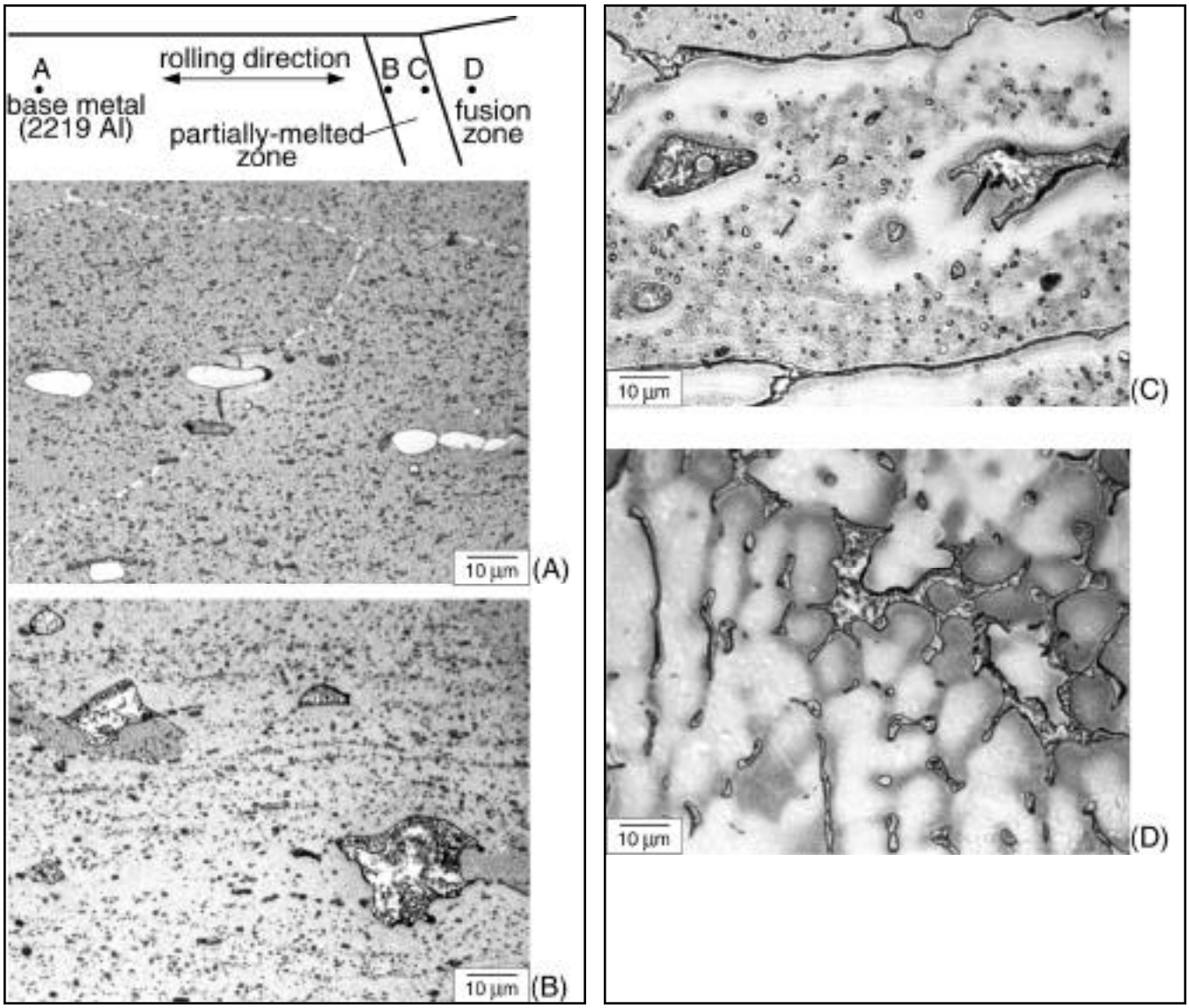

Fig. 7 — Optical micrographs. A — Base metal; B — edge of partially melted zone; C — partially melted zone; D — fusion zone.

particles are sharp at their intersections with the GBs. This indicates the eutectic liquid penetrates the GBs to some extent.

Partially Melted Zone

An optical micrograph of the PMZ is shown in Fig. 7C. The two largest eutectic particles are both coupled (α+θ) and divorced (θ). Most of the numerous tiny particles at isolated points within grains are divorced eutectic (θ). Most of the GB eutectic is divorced, though the thicker GB eutectic appears to be coupled.

One of the two eutectic particles is shown in the SEM micrograph in Fig. 8C. Again, the eutectic appears to be coupled in some areas and divorced in others. The divorced eutectic does not appear to be concentrating at the core and surrounded by the coupled eutectic. The GB eutectic appears divorced (θ) where it is thin and coupled (α+θ) where it is thicker.

In the PMZ, the maximum peak temperature during welding is above the eutectic temperature, T_E. At T_E, θ particles react with the α matrix to form the eutectic liquid. As temperature rises above T_E, the eutectic liquid lowers its Cu concentration along the liquidus line of the phase diagram (Fig. 2) by dissolving the surrounding α matrix of a much lower Cu content. Upon cooling, the hypoeutectic liquid solidifies first as Cu-depleted α and, finally, as the eutectic. In Fig. 7C, the light-etching phase along the lower side of the GB eutectic and surrounding the large eutectic particles is the Cu-depleted α phase that solidifies first. It gets darker near the eutectic, reflecting increasing Cu concentration. The EPMA results shown previously in Figs. 5 and 6 indicate a low Cu concentration of about 2 to 3% in the α phase.

If solid-state diffusion is negligible, the minimum Cu concentration of 2 to 3% in Figs. 5 and 6 suggests a local peak temperature of about 610°C during welding, according to the solidus line of the phase diagram. This peak temperature is not far below the 642°C liquidus temperature representing the peak temperature at the fusion boundary during welding. In other words, the areas corresponding to Figs. 5B and 6A are expected to be close to the weld. Back-scattered micrographs lower in magnifications such as Fig. 5A show the areas are about 100 μm away from the fusion boundary.

It is interesting to point out that the Cu-depleted α strip in the PMZ looks different in different types of micrographs.

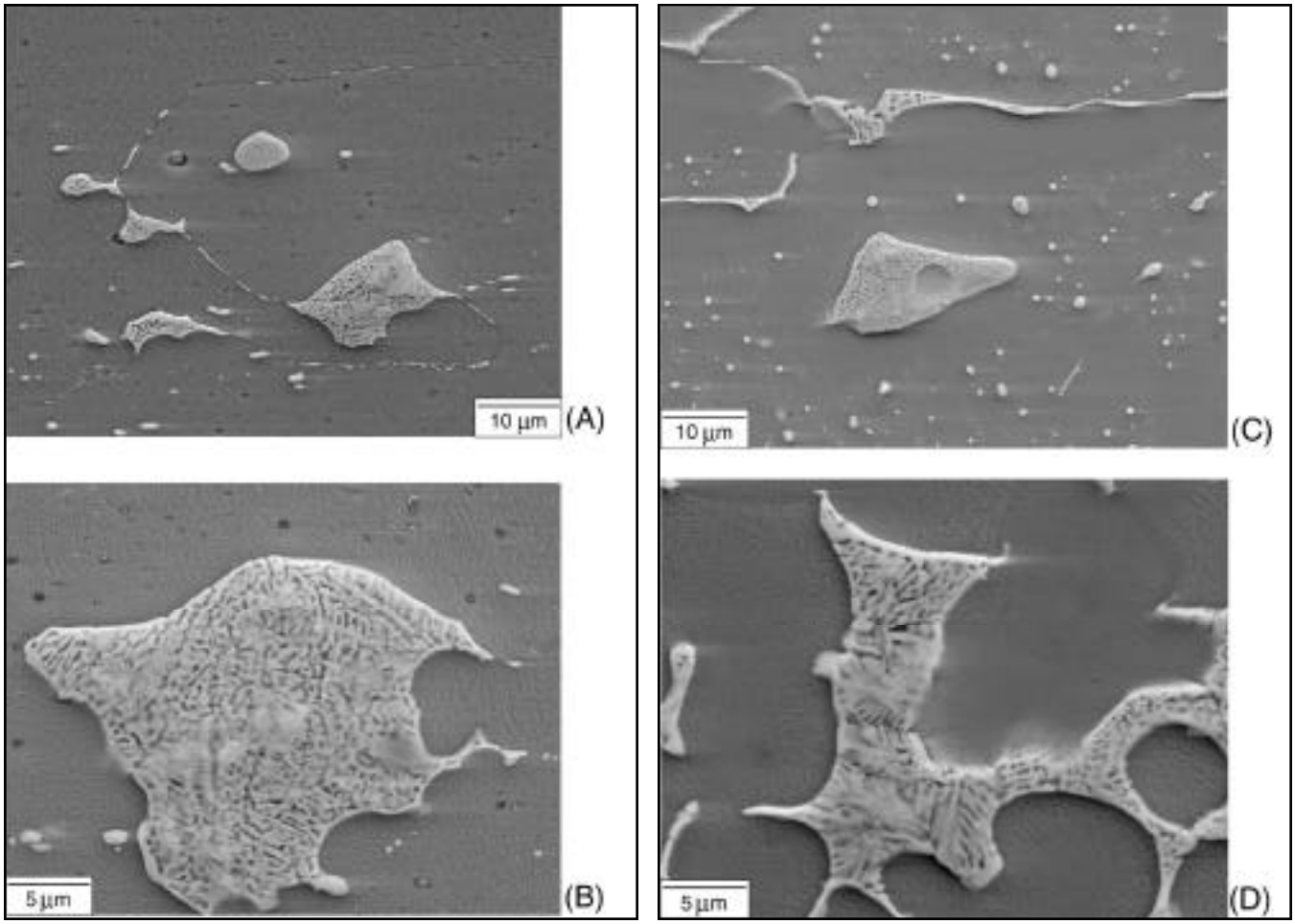

Fig. 8 — Scanning electron micrographs. A and B — Edge of partially melted zone; C — partially melted zone; D — fusion zone.

In an unetched EPMA electron micrograph (Fig. 5A), it appears dark. In an optical micrograph etched with a HF solution (Fig. 7C), it appears light. In a SEM micrograph etched with the same solution (Fig. 8C), it does not really stand out clearly.

Fusion Zone

In the fusion zone the peak temperature during welding is above the liquidus temperature of Al-6.3% Cu, which is about 642°C — Fig. 2. Since this is well above the melting point of θ (592°C), no θ can survive in the weld pool.

The optical micrograph in Fig. 7D shows the interdendritic eutectic in the fusion zone contains both coupled eutectic (α+θ) and divorced eutectic (θ). As already mentioned, divorced eutectic (θ) cannot be from residual θ that survives the heat of the welding process. The internal structure of the interdendritic eutectic is similar to that of the large eutectic particles in the PMZ — Fig. 7B, C. This further suggests divorced eutectic (θ) in the PMZ eutectic particles is not likely to be from residual θ. The cores of the dendrite arms, which solidify as the Cu-depleted α, appear light in color while the areas between the dendrite arms, which solidify later and have more Cu, appear darker. It is interesting to note some small and nearly round interdendritic particles appear to be divorced eutectic along.

The SEM micrograph of the eutectic in Fig. 7D is shown in Fig. 8D. Again, the interdentritic eutectic contains both coupled eutectic (α+θ) and divorced eutectic (θ).

Microhardness Testing

Figure 9 shows three Knoop microhardness indents in the PMZ: from the top down, one in the α strip, one on both the GB eutectic and the α strip, and one in the grain interior. The indent in the α strip is significantly wider than the other two, suggesting the α strip is much softer. The hardness levels are HK 60.9 in the eutectic-free α strip, HK 85.4 at the eutectic GB and HK 91.6 in the grain interior, which is full of small eutectic particles. Apparently, the Cu-depleted α phase is much softer than the eutectic. When the α phase is depleted in Cu, its strength decreases because of reduced solution strengthening.

Tensile Testing

As mentioned previously, tensile specimens were tested both with and without the reinforcement removed. With the reinforcement removed, cracking initiated in and propagated through the fusion zone. With the reinforcement kept, on the other hand, cracking initiated in the PMZ and propagated along the PMZ for some distance before stopping or continuing into the heat-affected zone. Leaving the reinforcement on the weld appears to cause a stress concentration effect and helps the crack to start at the toe. The results from the tensile

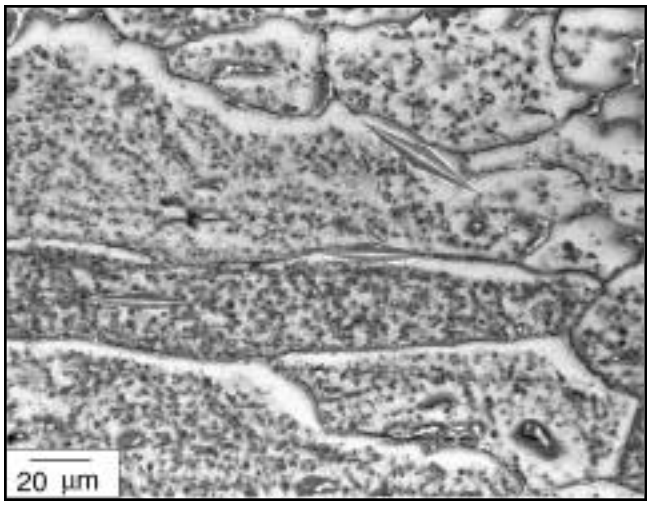

Fig. 9 — Microhardness indents in the partially melted zone.

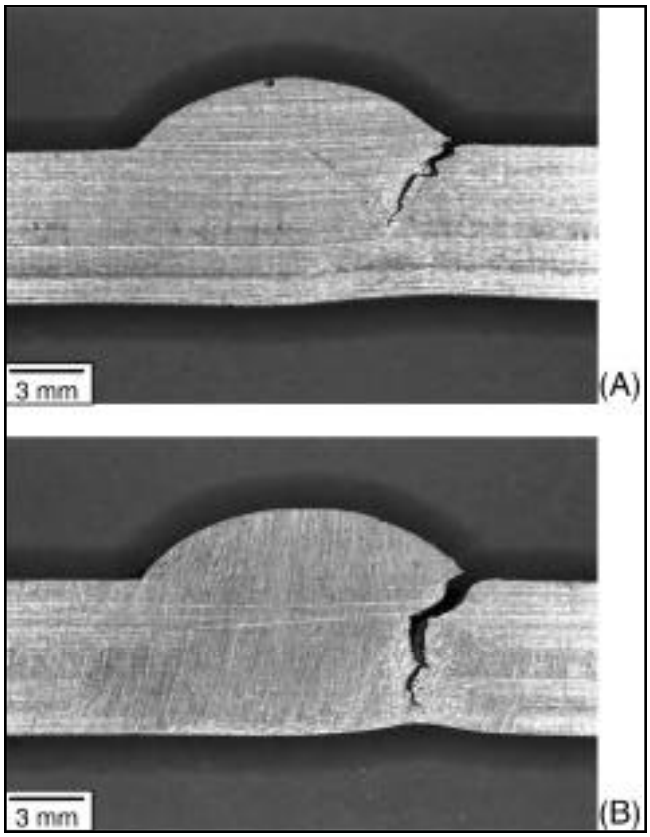

Fig. 10 — Tensile-tested specimens: A — Weld perpendicular to rolling direction; B — weld parallel to rolling direction.

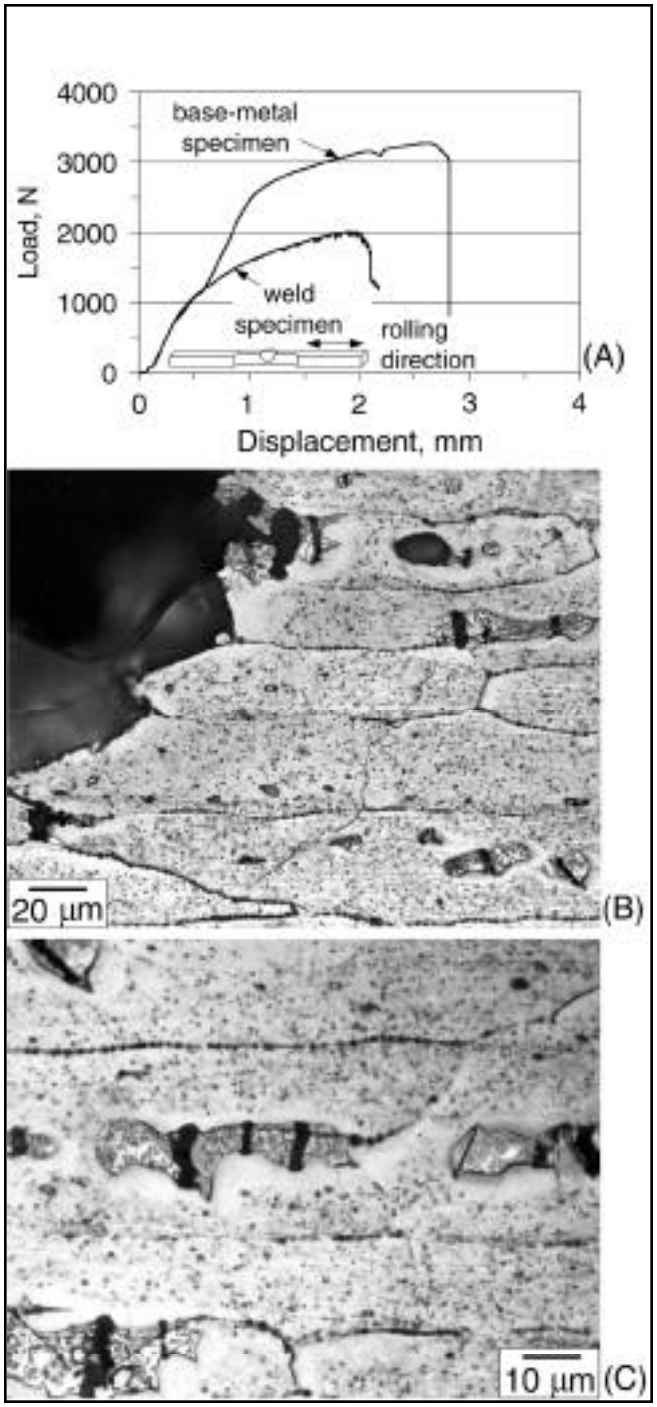

Fig. 11 — Tensile testing of weld perpendicular to the rolling direction: A — Load vs. displacement; B — micrograph near fracture surface; C — micrograph away from fracture surface.

specimens with the reinforcement kept will be discussed below.

Figure 10 shows two weld tensile specimens; one, perpendicular to the rolling direction (Fig. 10A) and the other, parallel (Fig. 10B). In both cases the crack runs along the PMZ, at least a good portion of it.

Weld Perpendicular to the Rolling Direction

The results of tensile testing for the weld perpendicular to the rolling direction are shown in Fig. 11. Figure 11A shows two curves of load vs. displacement, one for the weld specimen and the other for a base-metal specimen of the same rolling direction. The weld specimen is much lower in both strength and ductility than the base-metal specimen. In addition, the load fluctuates near the end of tensile testing.

An optical micrograph at the fracture surface of the weld specimen is shown in

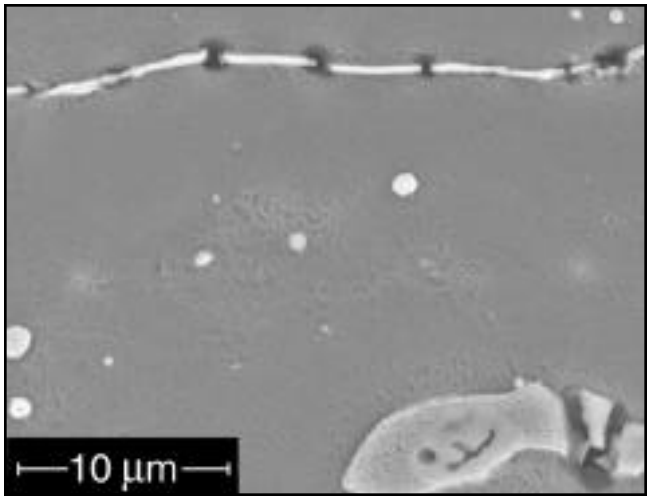

Fig. 12 — Scanning electron micrograph showing fracture of GB eutectic and a eutectic particle in the PMZ of a weld perpendicular to the rolling direction.

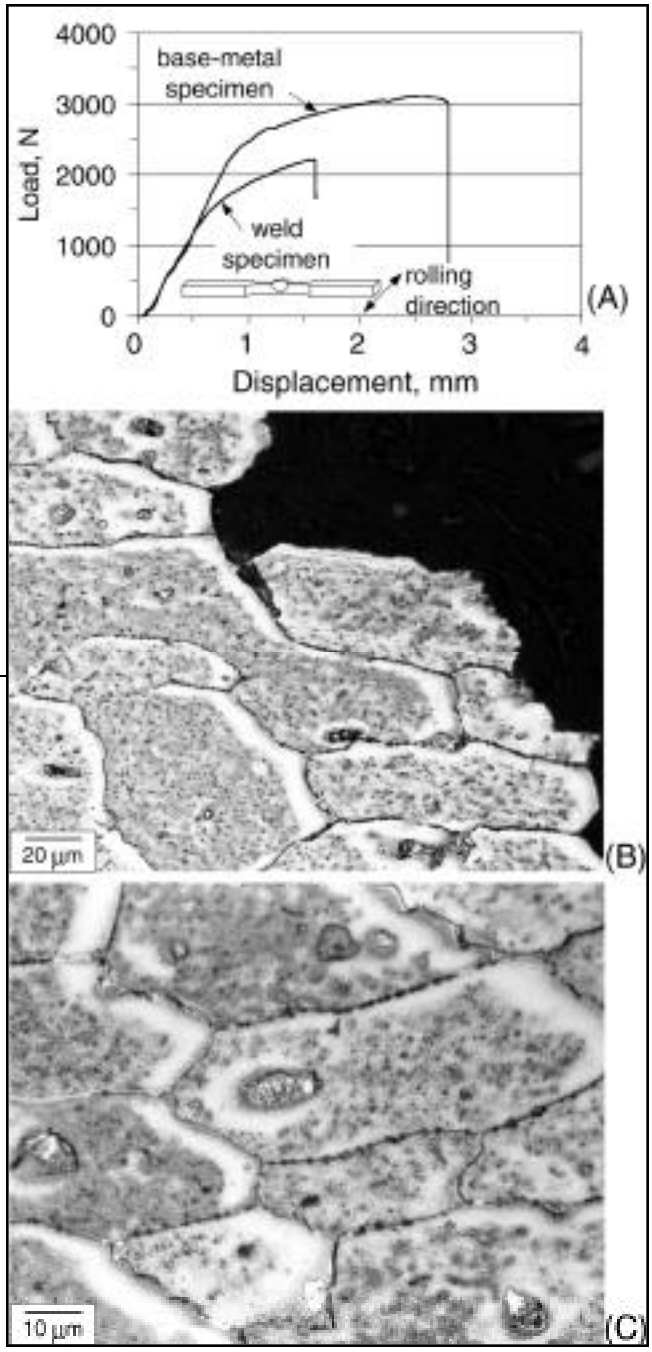

Fig. 13 — Tensile testing of weld parallel to the rolling direction: A — Load vs. displacement; B — micrograph near the fracture surface; C — micrograph away from the fracture surface.

Fig. 11B. Cracking appears to be both transgranular and intergranular. Fracture of the large eutectic particles is evident. Figure 11C is another optical micrograph in the PMZ at a higher magnification. Fracture is evident in both the GB eutectic and large eutectic particles. The SEM micrograph in Fig. 12 clearly shows the fracture of the GB eutectic. The grain boundary fractures in Fig. 11B and C are like those shown in Fig.12. It is likely the microcracks in the fractured eutectic particles and GB eutectic act as crack initiation sites, and that they propagate and eventually cause failure.

Weld Parallel to the Rolling Direction

Similar tensile testing results are shown in Fig. 13 for the weld parallel to the rolling direction. As shown in Fig. 13A, the weld specimen is again much lower in both strength and ductility than the base-metal specimen of the same rolling direction. However, as compared to the weld perpendicular to the rolling direction (Fig. 11A), the maximum load is slightly higher and the maximum displacement slightly lower. Also, the load does not appear to be fluctuating before it drops suddenly when the specimen begins to fail.

Figure 13B shows an optical micrograph at the fracture surface of the weld specimen. As compared to the weld perpendicular to the rolling direction (Fig. 11B), intergranular cracking seems to play a greater role. Figure 13C shows another optical micrograph in the PMZ at a higher magnification. It shows fracture of the GB eutectic, just like the weld perpendicular to the rolling direction (Fig. 11C), but not fracture of large eutectic particles.

Effect of Rolling Direction

The α phase next to the GB eutectic and surrounding large eutectic particles is solute-depleted (about 2 to 3% Cu) and is, therefore, weak and soft. The microhardness testing has already confirmed the Cu-depleted α phase is much softer than the eutectic. The α phase deforms easily under tensile loading because it is weak and ductile. The eutectic, on the other hand, is brittle and unable to deform. The fact that large eutectic particles and the GB eutectic stick to Cu-depleted α makes them susceptible to fracture under tensile loading.

The effect of the rolling direction is illustrated in Fig. 14. A single grain in the PMZ of the weld perpendicular to the rolling direction is shown schematically in Fig. 14A, and that in the weld parallel to the rolling direction in Fig. 14B. In both cases the brittle GB eutectic is bonded to the soft α strip. As the α strip elongates under tensile loading, the GB eutectic fractures.

In the weld perpendicular to the rolling direction (Fig. 14A), the large eutectic particles are elongated in the loading direction. This is because the prior-θ particles, which react with the surrounding α matrix and form these large eutectic particles, are often elongated in the rolling direction — Fig. 7A. Eutectic particles elongated in the tensile loading direction fracture more easily. The load fluctuations during tensile testing (Fig. 11A) are likely to be associated with the fracture of large eutectic particles — Fig. 11B, C.

In the weld parallel to the rolling di-

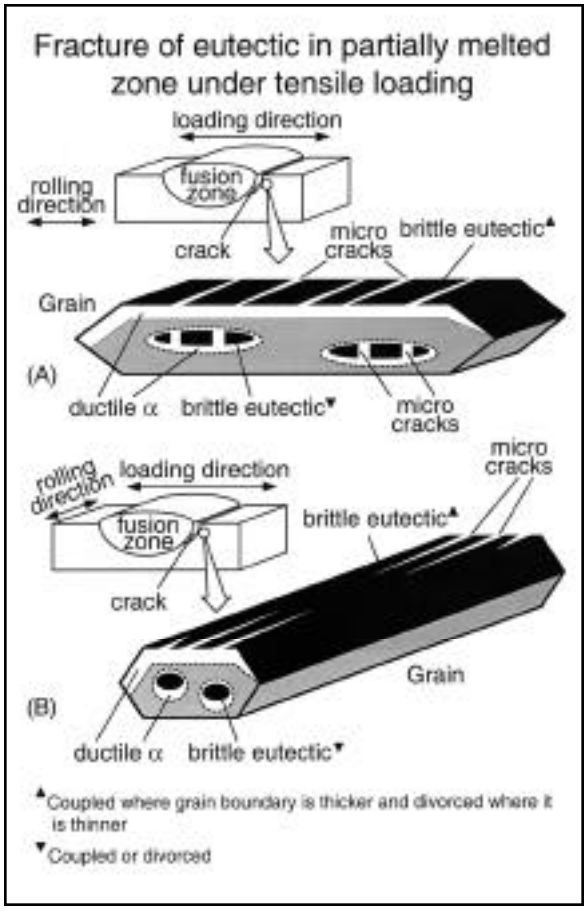

Fig. 14 — Fracture of the partially melted zone under tensile loading: A — Weld perpendicular to the rolling direction; B — weld parallel to the rolling direction.

rection (Fig. 14B), however, the large eutectic particles are less elongated in the loading direction and are, therefore, less likely to fracture. This is believed to be associated with the slightly less maximum displacement, slightly higher maximum load and the absence of significant fluctuations before failure.

Conclusions

The present study on welds of 2219 aluminum shows severe solute segregation can occur in the PMZ of an aluminum weld, resulting in a weak microstructure and poor mechanical performance. Liquation is evident both along GBs and at locations of prior-θ particles within grains. Severe Cu segregation occurs during solidification of the liquated material. Solidification begins with a Cu-depleted α phase (about 2 to 3 wt-% Cu) and finishes with a Cu-rich eutectic, which can range from normal eutectic (33 wt-% Cu) to divorced eutectic (55 wt-% Cu). The Cu-depleted α phase appears much softer than the eutectic. The PMZ is very much weakened by the microstructure of a weak ductile α phase and a brittle eutectic sticking to each other. The maximum tensile load and displacement are both well below those of the base metal before welding, and the GB eutectic fractures. A weld made perpendicular to the rolling direction behaves differently from a weld made parallel to it. The former shows a slightly lower maximum load, slightly higher maximum displacement and clearer load fluctuations. Its large eutectic particles are more elongated in the loading direction and are, therefore, easier to fracture.

Acknowledgments

This work was supported by the National Science Foundation under Grant No. DMR-9803589. The authors are grateful to Bruce Albrecht and Todd Holverson of Miller Electric Mfg. Co., Appleton, Wis., for donating the welding equipment (including the Invision 456P power source and the XR-M wire feeder and gun) and for their technical assistance during the study.

References

1. Kou, S. 1987. *Welding Metallurgy*. New York, N.Y.: John Wiley and Sons, pp. 29–59, 239–262.

2. Robinson, I. B. 1978. *The Metallurgy of Aluminum Welding.* Pleasanton, Calif.: Kaiser Aluminum Corp.

3. Gittos, N. F., and Scott, M. H. 1981. Heat-affected zone cracking of Al-Mg-Si alloys. *Welding Journal* 60(6): 95-s to 103-s.

4. Dudas, J. H., and Collins, F. R. 1966. Preventing weld cracks in high-strength aluminum alloys. *Welding Journal* 45(6): 241-s to 249-s.

5. Lippold, J. C., Nippes, E. F., and Savage, W. F. 1977. An investigation of hot cracking in 5083-0 aluminum alloy weldments. *Welding Journal* 56(6): 171-s to 178-s.

6. Metzger, G. E. 1967. Some mechanical properties of welds in 6061 aluminum alloy sheet. *Welding Journal* 46(10): 457-s to 469-s.

7. Steenbergen, J. E., and Thornton, H. R. 1970. Quantitative determination of the conditions for hot cracking during welding for aluminum alloys. *Welding Journal* 49(2): 61-s to 68-s.

8. Gibbs, F. E. 1966. Development of filler metals for welding Al-Zn-Mg alloy 7039. *Welding Journal* 45(10): 445-s to 453-s.

9. Young, J. G. 1968. BWRA experience in the welding of aluminum-zinc-magnesium alloys. *Welding Journal* 47(10): 451-s to 461-s.

10. Arthur, J. B. 1955. Fusion welding of 24S-T3 aluminum alloy. *Welding Journal* 34: 558-s to 569-s.

11. Huang, C., and Kou, S. 2000. Partially melted zone in aluminum welds — liquation mechanism and directional solidification. *Welding Journal* 79(5): 113-s to 120-s.

12. The Aluminum Association. 1982. *Aluminum Standards and Data*. Washington, D.C.: The Aluminum Association, p. 15.

13. American Society for Metals. 1986. *Binary Alloy Phase Diagrams*, Vol. 1. Metals Park, Ohio: American Society for Metals, p. 106.

14. Flemings, M. C. 1974. *Solidification Processing*. New York, N.Y.: McGraw-Hill, p. 95.

15. Joy, D. C. 1991. An introduction to Monte Carlo simulations. *Scanning Microscopy* 5(2): 329–337.

16. Collins, W. T., and Mondolfo, L. F. 1965. Divorced eutectic. *Transactions of the Metallurgical Society of AIME* 233: 1671–1676.

17. Kofler, A. 1965. Precipitation anomalies during isothermal crystallization from undercooled, binary organic melts. *The Journal of the Australian Institute of Metals* 10(2): 132–139.

18. Mondolfo, L. F. 1965. Nucleation in eutectic alloys. *The Journal of the Australian Institute of Metals* 10(2): 169–177.

19. Michael, F. X., Gigliotti, J. R., Colligan, A., and Grahan, L. F. P. 1970. Halo formation in eutectic alloy system. *Metallurgical Transactions* 1: 891–897.

20. Barclay, R. S., Niessen, P., and Kerr, H. W. 1973. Halo formation during unidirectional solidification of off-eutectic binary alloys. *Journal of Crystal Growth* 20: 175–182.

21. Bluni, S. T., Notis, M. R., and Marder, A. R. 1995. Nucleation characteristics and microstructure in off-eutectic Al-Zn alloys. *Acta Metallurgica et Materialia* 43(5): 1775–1782.